Mechanical Property and Microstructure of Linear Friction Welded WASPALOY

A. CHAMANFAR, M. JAHAZI, J. GHOLIPOUR, P. WANJARA, and S. YUE

The mechanical properties and microstructural evolution of WASPALOY joined by linear friction welding (LFW) were investigated in this study. *In-situ* temperature measurements using thermocouple probes indicated exposure of the weld area to a temperature of at least 1400 K (1126 °C). Based on electron backscatter diffraction (EBSD) mapping of the weldments, up to 50 pct reduction in γ grain size occurred within 0.9 mm of the weld interface as a result of dynamic recrystallization (DRX). Scanning electron microscopy (SEM) and transmission electron microscopy (TEM) studies revealed that progressive dissolution of γ' precipitates took place from the base metal to the weld interface, where almost no γ' precipitates were observed. Within 3.3 mm of the weld interface, the γ' dissolution significantly influenced the hardness profile measured across the extended thermomechanically affected zones (TMAZs). Investigation of strain distributions during tensile testing using the optical Aramis system revealed weak bonding at the edge of the weld due to oxidation. To extrude out oxide layers into the flash, increasing the axial shortening to higher than 1.2 mm is recommended.

I. INTRODUCTION

NICKEL-BASE superalloys have long been used in aerospace, power generation, chemical, and petroleum industries because of their superior mechanical properties and corrosion resistance at elevated temperature.[1,2] To join these alloys, mechanical fastening and fusion welding are usually employed. However, these conventional methods impair the properties of the joint. For example, mechanical joining of slotted blade/disk is associated with fretting fatigue damage;[3] melting and re-solidification processes in gas-tungsten arc, laser, or electron beam welding techniques result in welding defects such as microcracking, grain coarsening, and, consequently, the deterioration of mechanical properties such as ductility and fatigue strength.[4–8] Furthermore, conventional welding methods need filler wire, flux, or shielding gas during welding, which increase the complexity of the manufacturing as well as the costs.[9,10] To address these concerns, friction welding has been studied as an alternative joining method.

Linear friction welding (LFW) is solid state joining technology aimed at extending the current application of rotary friction welding to nonaxisymmetric components.[8] In friction welding, the temperature during the process does not reach the fusion point of the alloy;[11] thus, microcracking does not occur,[5] and filler metal addition or protective gas shielding are not necessary. LFW relies on the development of frictional heat at the interface by linear oscillation of one part relative to another while subjected to a pressure. This process consists of four distinct phases known as the contact phase, the conditioning phase (or friction), the burn-off phase, and the forge phase.[12] Once the components to be joined have been heated to a temperature that plasticizes the material at the interface, the oscillating part is stopped in an aligned position with the stationary part. Then, the axial load is maintained or increased to consolidate and bond the two parts together. During the process, some of the plasticized material is expelled to the sides as flash. The bonding mechanisms in the LFW process can be summarized as follows:

(a) viscoplastic flow and intermixing of the interface material from two weld halves as a result of under pressure oscillation and forging,
(b) local micromechanical bonding (interlocking of asperities),
(c) high-temperature diffusion: the transfer of atoms across the interface facilitated by frictional heat,[4,13,14] and
(d) development of clean surface due to separation of oxide layers, electron sharing, and metallic bonding.[15]

The resulting joint has a relatively limited thermomechanically affected zone (TMAZ) due to localized heat generation and short joining time.[11] LFW has been considered for the manufacturing of blisks (blades to disk integral assemblies machined from solid forged billets) used in land-based gas turbines and aero-engines

A. CHAMANFAR, PhD Candidate, is with the Department of Mining and Materials Engineering, McGill University, Montreal, QC, Canada H3A 2B2 and is also a Visiting Worker, Aerospace Manufacturing Technology Center (AMTC), Institute for Aerospace Research (IAR), National Research Council of Canada (NRC), Montreal, QC, Canada H3T 2B2. Contact e-mail: ahmad.chamanfar@mail.mcgill.ca M. JAHAZI, Adjunct Professor and S. YUE, Professor, are with the Department of Mining and Materials Engineering, McGill University. J. GHOLIPOUR, Research Officer and P. WANJARA, Group Leader, are with the AMTC, IAR, NRC.

on materials such as steel, titanium alloys, and nickel-based superalloys.[16,17] The high joint integrity and low distortion of welded components along with 20 to 30 pct weight savings, associated with the removal of the fir tree in conventional blade to disk assembly, are some of the potentials of the LFW process.[3,16] Moreover, the mechanical properties can be readily tailored to meet the required operating temperatures by LFW dissimilar alloys (e.g., different grades of superalloys[4,18] and Ti alloys[19] as well as different microstructures such as polycrystalline to single crystal[20]), since the segregation of solutes and alloying elements is limited in LFW due to the solid state nature and short duration of the process. Finally, although friction welding needs higher capital expenditures in comparison to conventional welding techniques, the high level of automation and reproducibility make it a highly competitive process[10,21] and an excellent alternative manufacturing technique for critical components in the next generation compressors and turbines.

WASPALOY* is a nickel-base superalloy commonly

*WASPALOY and INCONEL are trademarks of Special Metals Corporation, New Hartford, NY.

used as blade and disc material in jet engines with excellent high-temperature mechanical properties[22] that are mainly due to the presence of γ' precipitates, Ni_3 (Al, Ti), dispersed in the nickel matrix (γ).[23] The size, composition, morphology, and the kinetics of γ' precipitation are critical factors in determining the elevated temperature capabilities of WASPALOY. For example, in nickel-base superalloys, a γ' subsolvus solution heat treatment is applied after hot deformation to produce primary γ' particles (1 to 5 μm) at the grain boundaries, with the objective of preserving a fine grain size by preventing grain growth.[24] Intragranular secondary (50 to 500 nm) and tertiary (10 to 50 nm) γ' precipitate at early and late stages, respectively, during cooling from the solution temperature.[24,25] Because the microstructure of the nickel-base superalloy is influenced by the thermomechanical processing (TMP) condition, it is of paramount importance to better understand the evolution of the γ' characteristics during LFW processing.

Little data have been published on microstructure evolution during LFW of nickel-based superalloys and even less on γ' evolution and its impact on mechanical properties of welded joint in WASPALOY. Work carried out on rotational friction welding, also called inertial friction welding (IFW), of nickel-based superalloys[4,25] indicated partial or full dissolution of γ' in the weld area as a result of the thermal cycle experienced during the welding. LFW of INCONEL* 718 was reported to result in a maximum loss of strength (from 334 to 250 HV) at the bond interface as well as dynamic recrystallization (DRX) in a 3-mm narrow band of the TMAZ.[26,27] A study focused on the determination of residual stress in linear friction welded WASPALOY reported the presence of large tensile stresses in the weld area.[28]

In light of the limited information available, the main objective of the present study was to quantify and explain the evolution of the microstructure, particularly with regard to γ' and grain size evolution, and its impact on mechanical properties under various LFW process conditions of WASPALOY. This study specifically highlights the influence of frequency, amplitude, and pressure during oscillation to achieve a sound joint. The in-process temperature was recorded and the characteristics of the welds were evaluated by optical microscopy (OM), electron backscatter diffraction (EBSD), scanning electron microscopy (SEM), transmission electron microscopy (TEM), microhardness testing, and tensile testing.

II. EXPERIMENTAL PROCEDURE AND MATERIALS

Rectangular blocks with dimensions of 13 mm in length (L), 11 mm in width (W), and 18 mm in height (H), as shown in Figure 1, were prepared by electrodischarge machining (EDM) from an as-received WASPALOY disc containing (wt pct) 17.08Cr, 12.87Co, 1.00Fe, 4.12Mo, 3.35Ti, 1.07Al, 0.07B, 0.01Zr, and 0.04C. The disc was in the standard heat-treated condition, solution heat treated and double aged. The γ' solvus temperature was determined to be about 1303 K (1030 °C) by conducting some solution heat treatment experiments. Shen et al.[29] reported this temperature to be 1300 K (1027 °C) for WASPALOY with Al and Ti contents of the present study alloy. After cleaning the surfaces to be welded with acetone, LFW was carried out with the oscillation applied perpendicular to the $H \times W$ cross section (Figure 1) using an MTS LFW Process Development System (PDS, MTS Systems Corporation, Eden Prairie, MN). This system consists of two
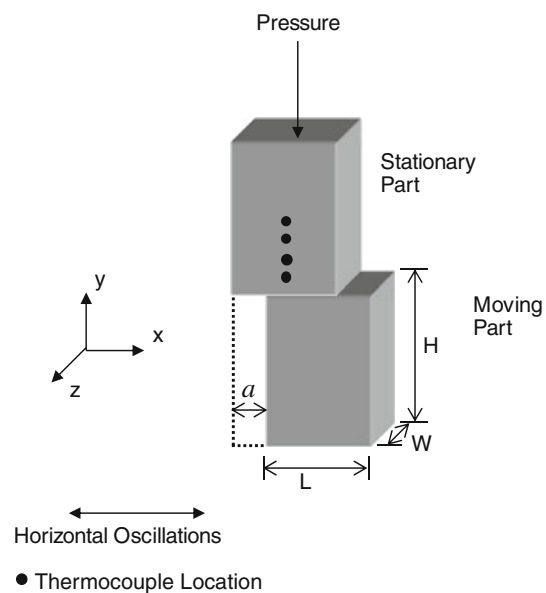

Fig. 1—Sample geometry, LFW process principles, and the location of the thermocouples.

Table I. LFW Processing Conditions Used in the Present Study

Specimen ID	f (HZ)	a (mm)	P (MPa)	SPI (kW/m^2)
W1	40	2	50	637
W2	60	2.5	70	1671
W3	80	3	70	2674
W4	80	3	90	3438

hydraulic actuators: the in-plane actuator that oscillates the lower work piece in the horizontal direction and the forge actuator that applies a downward load on the stationary work piece. More details about the technical specifications of the MTS LFW PDS system are provided in Reference 30. No protective atmosphere was used and all the experiments were conducted at room temperature.

In the present research, the influence of the critical process parameters, a, amplitude of oscillation (mm); f, frequency of oscillation (Hz); and P, pressure during oscillation (MPa) on flash morphology, microstructure, and mechanical property of the welded samples, were investigated. The experimental plan used in the current study is presented in Table I. For all specimens, the stabilization or forge pressure was the same as the pressure during oscillation. The LFW parameters were first selected based on the data reported in the open literature for other nickel-based superalloys.[26,27] To ensure the accuracy and reliability of the results, duplicate welds were performed for each set of process parameters. The specific power input (SPI) parameter, as indicated in Eq. 1, has been proposed and used by some authors as a means to illustrate the combined effects of the process parameters:[16,31]

$$\mathrm{SPI} = \frac{afP}{2\pi} \qquad [1]$$

Table I also shows the SPI value for different processing conditions used in the present study.

Welded samples were sectioned through a plane parallel to the (x, y) plane indicated in Figure 1 at midwidth, using a precision abrasive alumina oxide cut-off wheel. Conventional grinding and polishing procedures were used to prepare the samples for microhardness testing and microstructural examination. Microhardness tests across the weld region were performed on a grid of five lines parallel to the y-axis (Figure 2) under a load of 500 g and a dwell time of 15 seconds using a Struers Duramin-A300 Vickers microhardness testing machine (Struers Company, Ballerup, Denmark). Measurements were carried out from the weld to a distance of 9 mm on either side of the interface well within the base metal zone. The axial distance of the indentation lines along the x direction was 2 mm, as shown in Figure 2. Also, on each line in the y direction, measurement locations were spaced greater than 5 times the indentation diameter. For each LFW condition, 60 indentions on every line were measured and the reported results are the average of the five microhardness test profiles.
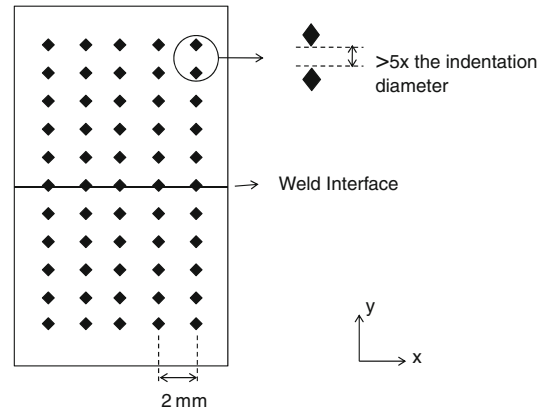

Fig. 2—Schematic of the five indentation lines used for microhardness measurement.

Tensile tests were carried out at a speed of 0.03 mm/s on flat rectangular test pieces obtained by cutting the welded samples in half, parallel to the length, at the middle of the width (W/2 in Figure 1); one of the halves was tested. The MTS universal tensile testing machine used in this study was integrated with an Aramis system (GOM Optical Measuring Techniques, Braunschweig, Germany), which is a noncontact three-dimensional optical image correlation system that captures digital images during the test to measure automatically the amount of deformation. The system consists of two CCD cameras capable of capturing 15 frames per second (fps) and requires a speckle pattern, consisting of random black dots on a white background, applied on the surface of the sample to calculate the strain distribution. In the current study, 2 fps was used for the tensile testing. Captured images were analyzed by the Aramis dedicated software, and strain distributions across the weld were obtained for every frame or deformation stage.

Microstructure evolution was investigated by OM, EBSD, high resolution SEM, and TEM. Final polishing of the EBSD samples was performed with a vibratory polisher for 12 hours. Grain size evolution was determined by analyzing the EBSD maps acquired for 13 areas from the weld interface to the base metal. During EBSD mapping, the electron beam was scanned over the polished surface of the sample while the sample was tilted 70 deg to the backscatter detector of a PHILIPS**

**PHILIPS is a trademark of Philips Electron Optics, Eindhoven, Holland.

XL-30 field emission gun–SEM (FEG-SEM), which was equipped with an TSL EBSD acquisition system (Philips Electron Optics, Eindhoven, Holland) and operated at an accelerating voltage of 20 kV. EBSD patterns were detected by a CCD camera with background subtracted by TSL OIM Data Collection 4 software (Philips Electron Optics, Eindhoven, Holland). The EBSD maps were generated from the weld interface to a distance of 4 mm with a scanning step size of 0.2 to 0.7 μm,

depending on the grain size. A line scan in the EBSD was employed to obtain an estimate of the grain size, which was then used to select the appropriate step size. The γ grain size was obtained from the EBSD maps. For the OM studies, the polished samples were ultrasonically cleaned and then etched by immersion in a solution composed of 60 mL HCL, 40 mL HNO_3, and 40 mL CH_3COOH.[32]

A high resolution S-4700 FEG-SEM at an accelerating voltage of 15 kV in secondary electron (SE) mode was used to study the morphology, distribution, size, and volume fraction of the γ' phase from the weld interface to the base metal. To this end, the samples were electroetched at 0.1 A and 3.0 V for 1 second in a solution of 0.4 g CrO_3, 42 mL H_3PO_4, and 2.5 mL H_2SO_4.[33] This etchant dissolves the γ matrix from the polished surface while leaving γ' precipitates undamaged. To reveal very fine γ' precipitates, a minimum electroetch time of 1 second was selected, since the secondary γ' content was found to decrease (dissolve) with increasing electroetch time from 1 second to 5, 7, or 10 seconds. Microhardness indentation marks were used as references for capturing images at predetermined locations from the weld interface. Furthermore, in order to minimize statistical variation in the γ' volume fraction determination, six images at low magnification (25 k) and six images at high magnification (60 k) were captured for each location from the joint interface. The primary γ' volume fraction was determined from low magnification images, while those of secondary γ' particles were obtained from high magnification images.

The γ' size was measured using the Clemex image analysis software (Clemex Technologies Inc., Longueuil, QC, Canada). The volume fraction of the γ' was determined based on ASTM E 562-02 standard.[34] The average γ grain size for each EBSD map was given by EBSD software. For γ grain size, γ' size, and volume fraction determinations, at least six micrographs were examined to increase reliability of the data and obtain statistically representative results.

For TEM investigation, samples were cut from the welds and ground to a thickness of about 80 to 100 μm. Discs with 3-mm diameter were punched from the thinned samples. The discs were further thinned by jet polishing carried out at 233 K (–40 °C), 0.6 A, and 50 V in a solution consisting of 20 vol pct perchloric acid and 80 vol pct methanol. To remove any remaining electropolish film, the discs were ion beam milled. TEM was done on a PHILIPS CM200 machine at 200 kV.

In order to measure the variation of temperature in TMAZ during welding, additional LFW experiments were carried out. Blind holes with 1.3-mm diameter were drilled at midlength ($L/2$) of the top stationary part perpendicular to the (x, y) plane at four different locations from the weld interface: 1.5, 2.8, 4.2, and 5.5 mm (Figure 1). The depth of these holes was set to the middle of the width ($W/2$). A Chromel Alumel K type thermocouple (Omega Engineering Inc., Stamford, CT) with spark welded tip was embedded in each hole and fixed with thermoplastic adhesive in order to eliminate any displacement of the thermocouple junction during oscillation. Thermocouple probes were made from 0.1-mm-diameter thermocouple wires, the finest commercially available gage, to minimize the response time. Furthermore, because an exposed junction thermocouple has the fastest response, special precautions were taken to prepare the junction to avoid ground contact; a high-temperature fiberglass spacer tube was employed before welding the tip to isolate the bare thermocouple wires. Signals were recorded constantly during the welding by the data acquisition software at a rate of 90 points per second. For each location from the interface in the y-direction, the temperature was measured at the center of the x-y plane (Figure 1) of the LFW sample.

III. RESULTS AND DISCUSSION

A. Macroscopic Examination

Visual examination of the flash morphology (Figure 3) revealed that only the weld with the highest SPI exhibited a symmetric flash. For lower SPIs, asymmetric flash formation was observed with the volume of the flash being higher in one of the weld halves. This behavior might be due to different temperature distributions on each side of the interface and a greater extrusion of the plasticized and softened layer from one half.

Note that for the asymmetric samples, the extruded material was "incomplete," in that it did not extend to all the corners (arrowed in Figures 3(a) through (c)), suggesting that bonding may not be entirely integral at the interface in these specimens. In contrast, for the W4 specimen (Figure 3(d)), the top and bottom flashes were "complete," which suggests that the entire area of the interface was plasticized during the LFW process, resulting in satisfactory bonding.[16] Subsequent examination of the weld by nondestructive liquid penetrant technique and optical microscopy revealed no microcracks or microvoids in W4. However, the integrity of the weld interface was further investigated by conducting a tensile test, as described subsequently. From the preceding observations, there appears to be a critical power input that is necessary to obtain a "complete" weld. In this work, this critical value was determined to be between 2674 and 3438 kW/m^2.

The extruded materials from the weld halves were separated from each other; a double flash developed, as shown in Figure 3. In previous linear and rotary friction welding studies, it was reported that flash morphologies depend on material type: Ti alloys exhibited a single joined flash,[30,35] while other alloys such as plain carbon steels,[36] stainless steels,[37] Al alloys,[38] and INCONEL 718[27] showed a double flash extruded from each weld half. The results obtained in the present study confirm the occurrence of a double flash morphology in WASPALOY.

B. Microhardness Measurements

Microhardness was used in this investigation as an indication of the variation in mechanical properties across the weld. Figure 4 depicts microhardness
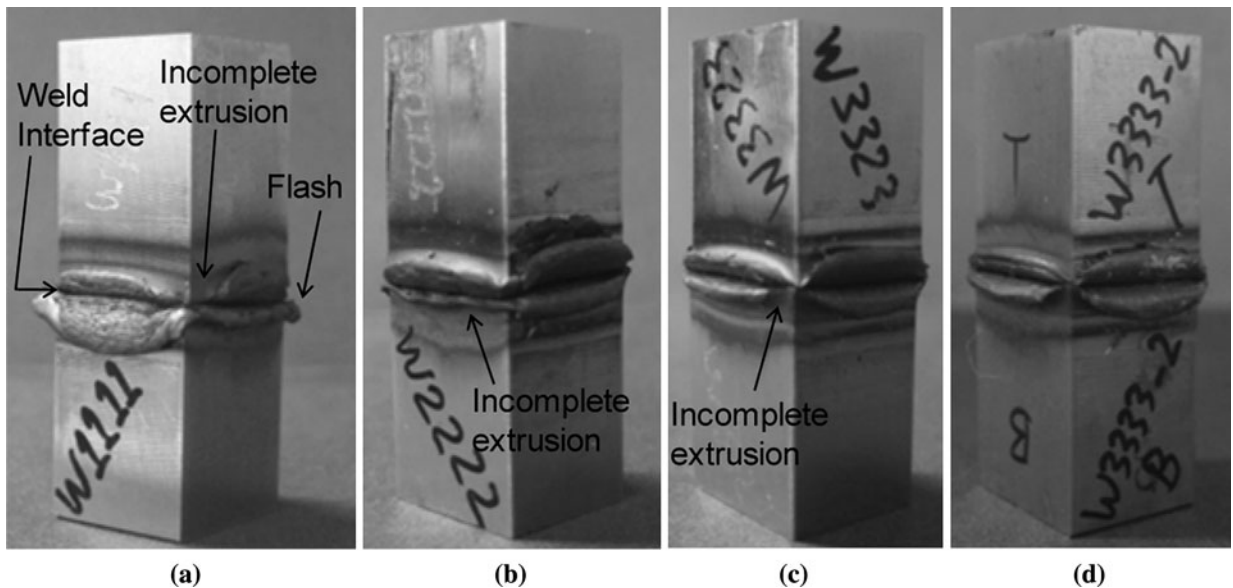
Fig. 3—Photographs of the linear friction welded specimens: (*a*) W1, (*b*) W2, (*c*) W3, and (*d*) W4.
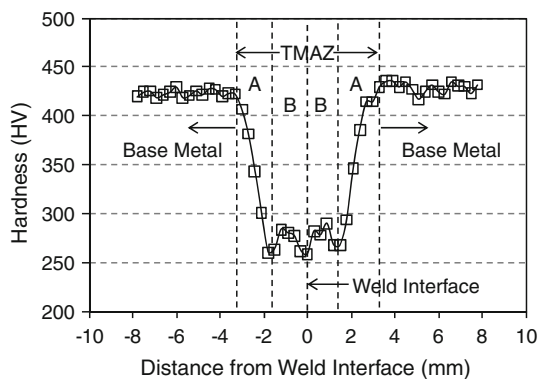

Fig. 4—Variation of the Vickers microhardness across the weld in the W4 specimen presenting the overall loss of strength in the TMAZ. The sample was welded in the as-received condition (aged).

Fig. 5—Microhardness profile of the W2 specimen.

variations in the W4 specimen. Based on this figure, the width of the TMAZ was determined to be 6.6 mm (3.3 mm on either side of the interface). It can also be seen that the hardness of the base metal drops from 426 to 258 HV at the weld interface. In the TMAZ, two symmetrically distinct regions (*A* and *B*) can be identified. In region *A*, the hardness falls quickly from 426 to 265 HV. In region *B*, the hardness initially increases from 265 to 284 HV at ±0.9 mm from the weld interface and then decreases to 258 HV at the interface.

The observed symmetry in microhardness profile with respect to the weld interface suggests that the material adjacent to the interface is thermomechanically affected in the same way regardless of which half is the stationary or the oscillatory work piece. The small scatter in the base metal hardness can be related to the indentation size and the grain size.[39] The base metal grain size was 15.1 μm, while the average indentation size was 47 μm. Thus, for the base metal, hardness was measured on a few grains resulting in small discrepancies in the hardness measurements (426 ± 5 HV). In contrast, in
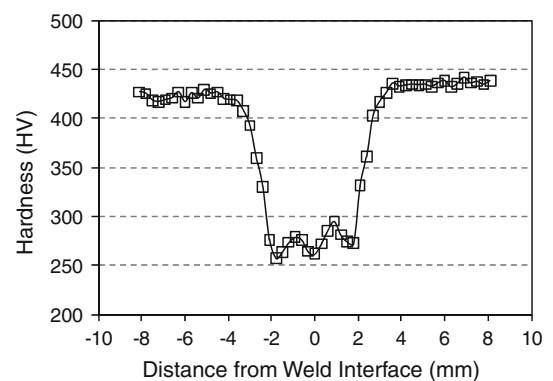
the weld area, the grain size was smaller (about 7.5 μm, as described in Section III–E) and the indentation was larger (~60 μm) due to the lower hardness, and thus each hardness indent sampled a much higher number of grains, leading to lower scatter in the results. Also, a slight hardness difference was observed for the base metal region of the two weld halves that is probably due to variations in the TMP conditions across the disk from which the specimens were machined. It is interesting to note that other welded samples (W1, W2, and W3) exhibited much higher hardness asymmetries compared to W4 (*e.g.*, W2 shown in Figure 5). This level of asymmetry may explain why asymmetric flash was observed in W1, W2, and W3.

The variation of the TMAZ width as a function of SPI is shown in Figure 6. The TMAZ width was estimated from the hardness profiles. It can be noted that the TMAZ width depends on two opposing effects: (1) SPI level contributing to the heating of the interface material and (2) the applied forge pressure that influences the amount of flash. At the beginning, the TMAZ width increased with SPI (W1 to W2 in Figure 6). With a further increase in SPI, the TMAZ width decreased

(W3 in Figure 6), since more heating and softening occurred in W3 relative to W2; thus, there was more extrusion of the softened high-temperature material from the weld interface as flash at a constant pressure of 70 MPa. The W4 specimen exhibited the smallest TMAZ width, because the highest SPI and pressure were applied.

C. Elongation Distribution across the Weld

Distribution of the major strain during tensile testing across the weld was determined by the Aramis system. Figure 7 displays the elongation or major strain distribution at different stages during tensile testing of W4 specimen; the weld interface was perpendicular to the tensile direction. Note that the color scale calibration changes as the test proceeds; therefore, red always indicates the highest strain, but the absolute value changes.
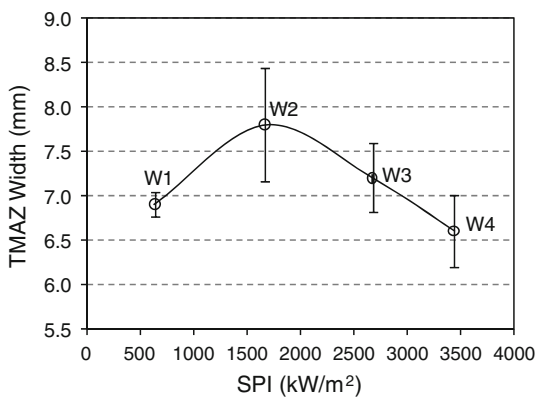

Fig. 6—TMAZ width as a function of SPI determined from microhardness profile of each welded sample. The standard deviations of measurements are shown as error bars.

Figure 7(a) displays the strain distribution at the beginning of the test; it can be seen that higher elongation occurred in the gripped region. However, the strain in the gripped area is about 1 pct, which is negligible and is either due to the edge effect in the paint or due to the gripping force applied to the sample. As deformation progresses, strain localization is observed at the edge of the weld interface (Figure 7(b)). SEM and energy dispersive X-ray spectroscopy (EDS) analysis of these peripheral regions at weld extremities revealed the presence of Ti, Cr, Al, and Ni oxides, indicating that they were probably not ejected during the final phase of the LFW process. A clear lack of joint integrity at the edges compared to the central region of the weld was observed with further deformation, as can be seen in Figures 7(c) through (f). Microstructural examination confirmed the higher presence of metal oxides and the resultant weak bonding with increased straining. In Figure 7(f), there is a ringlike higher strain region at the central area of the weld, which might be a result of the cracks developing different plastic zones at the crack tips. Figure 7(g) is indicative of deformation localization in the central region of the weld leading to the highest elongation values, 16.5 pct, measured in this zone (Figure 7(h)). The weld plane was the weakest area in the LFW sample, partly because of the weak bonding at the edges of the weld and partly because the hardness was lowest, as was revealed by the microhardness measurements in Figure 4.

Though the application of shielding gas during LFW may reduce the extent of oxides at weld periphery, optimization of the LFW parameters to increase the amount of extruded flash has been observed to be effective in achieving complete bonding across the interface for other nickel-based superalloys studied by the present authors. For instance, conducting the oscillation for longer periods of time (>4.4 seconds) to expel any remaining oxides as flash and thereby
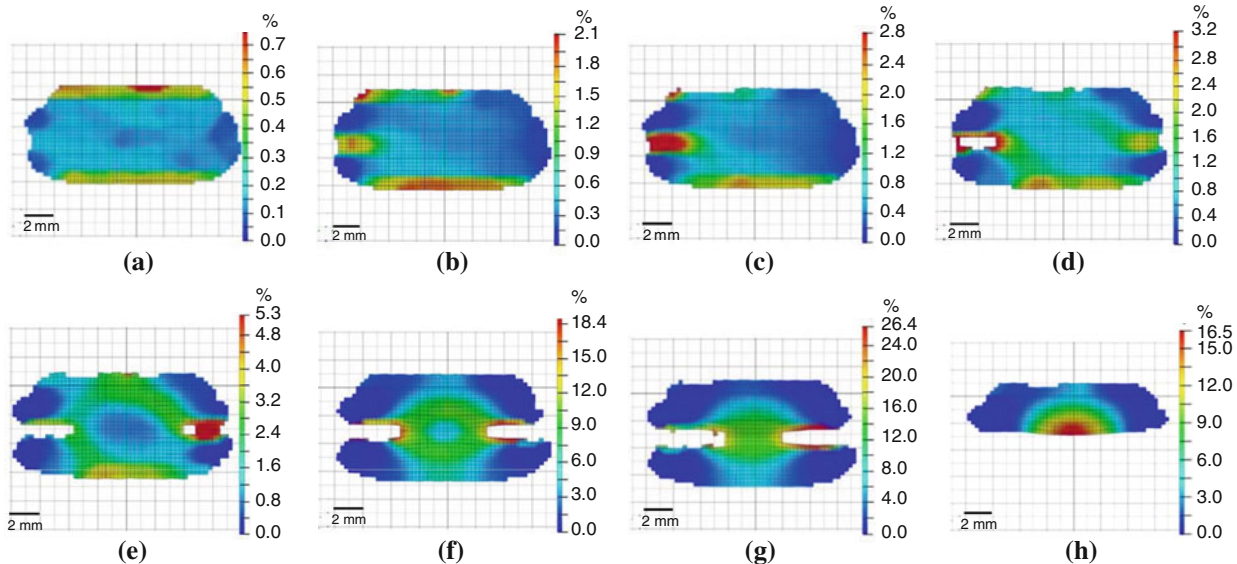

Fig. 7—Strain distribution across the weld in the W4 sample: (a) 5.5 s, (b) 12 s, (c) 13.5 s, (d) 15 s, (e) 16 s, (f) 22.5 s, (g) 27 s, and (h) 34 s after the start of tensile testing.

improving the bonding in the weld periphery is a possible solution, although this may also generate more oxide. Perhaps a better solution is to increase the axial shortening beyond what was used for W4, *i.e.*, 1.2 mm, to achieve this goal. Finally, the development of residual stresses in the linear friction welded assembly is an important consideration, because it affects the mechanical behavior and it may also cause distortion. Determination of residual stresses in the linear friction welded WASPALOY studied in the present work is under investigation.

D. Temperature Measurements during LFW

The temperature evolution during the LFW process was determined from the data recorded from the thermocouples. Figure 8 presents the recorded temperatures at different locations from the weld interface for the W4 specimen. Due to the nature of the process, a very sharp temperature increase was observed in the weld region. At the initial distance of 1.5 mm from the interface, a heating rate of 368 ± 140 K/s was recorded. As the thermocouple was placed further from the interface the heating rate decreased. The temperature increased up to a peak value and then dropped quickly at the end of the welding process. At the 1.5-mm location, the cooling rate was 62 ± 4 K/s, while for other locations, the rate was slower. In fact, at the end of the joining process, the interface material cooled very rapidly due to flash formation and heat dissipation into

the surrounding material. The peak temperature achieved for each measurement location is shown in Table II. These data clearly show that the highest temperature encountered was at the interface. Grant *et al.*[40] predicted similar profiles by finite element modeling of IFW for RR1000 nickel-base superalloy.

The sharp temperature increase and the short time exposure at high temperature along with rapid cool-down at the end of the process resulted in severe microstructural changes across the weld. These mainly include variation in γ grain size and γ' dissolution, as are discussed in Sections III–E and F.

In Figure 9, the variation of load, stroke, and temperature with time is shown for W4 specimen. In the contact phase, region (1), the forge actuator moved downward at a rate of 0.1 mm/s; when the pressure reached 90 MPa, it was held for 3 seconds to stabilize the positions of the fixtures and the specimen. At the end of this phase, the pressure was decreased to 20 MPa, to ensure that contact was always made. As expected, in the contact phase, no variation in the temperature of the weld parts occurred. In the conditioning phase, region (2) in Figure 9, the desired pressure was reached "instantaneously," within 0.2 seconds, to 90 MPa and oscillation of the lower part against the upper one was applied at a frequency of 80 Hz and amplitude of 3 mm for a very short period of time, 0.2 seconds, to remove surface oxides. At the end of this phase, the axial shortening was about 0.3 mm with insignificant temperature increase of the work pieces. In the burn-off phase, region (3), the oscillation continued with the same frequency and amplitude of the previous
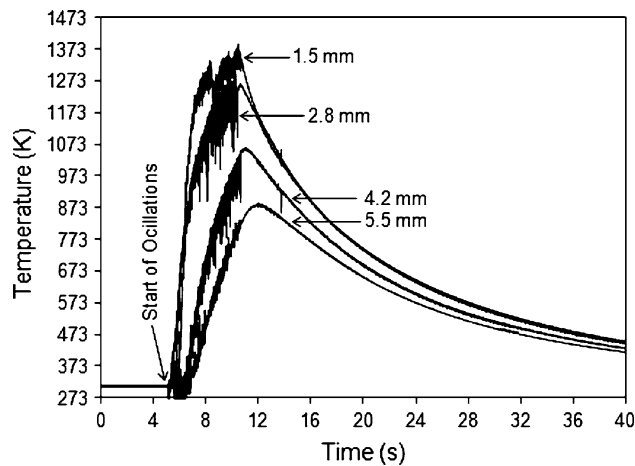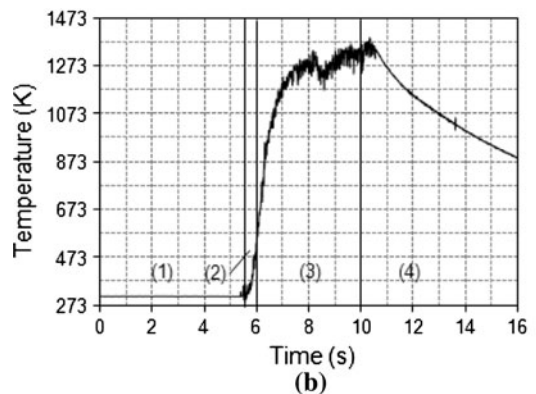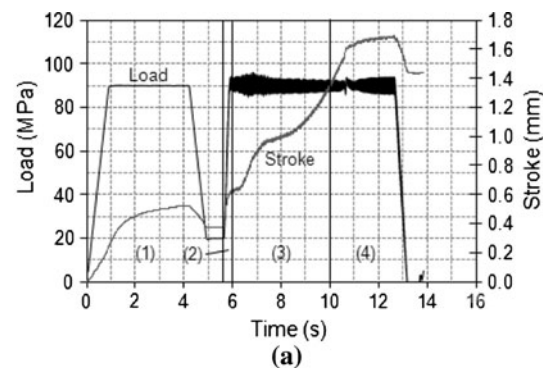

Fig. 8—Variation of temperature during LFW for the W4 specimen with initial thermocouple position at 1.5, 2.8, 4.2, and 5.5 mm from the interface.

Table II. Peak Temperature at Different Locations from the Weld Interface in W4; the Standard Deviations Are Also Shown

Initial Location from Interface, mm	Peak Temperature K, (°C)
1.5	1400 ± 9 (1126 ± 9)
2.8	1257 ± 31 (984 ± 31)
4.2	1083 ± 30 (810 ± 30)
5.5	913 ± 35 (640 ± 35)

Fig. 9—Variation of (*a*) load and stroke and (*b*) temperature at initial position of 1.5 mm, as a function of time during the LFW process.

phase until a stroke of 1 mm from the initial contact position was achieved.

During the burn-off phase, where high frequency oscillation or extrusion occurred under high pressure, the temperature increased to about 1313 K (1040 °C), and then dropped to about 1173 K (900 °C) and again increased to about 1353 K (1080 °C). The observed fluctuations around 1273 K (1000 °C) might be due to the failure of the thermocouple junction, rejoining of the two thermocouple wires, or displacement of the thermocouple during the harsh conditions rather than specific metallurgical phenomena. Finally, in order to stabilize bonding, the two joint halves were held together in an aligned position, and the pressure was maintained at 90 MPa, which led to a stroke increase of about 0.3 mm. This position was held for at least 2 seconds in the last phase, region (4). At the beginning of this stage, there was a modest temperature increase from 1353 to 1400 K (1080 °C to 1126 °C) due to adiabatic heating from plastic working of the material, since this increase in temperature corresponds to the increase in the stroke. The influence of plastic work heat on the increase in the work piece temperature is reported by other researchers. For instance, Brand et al.[41] reported a 323 K (50 °C) temperature increase during hot compression of INCONEL 718 due to plastic work at deformation temperatures of 1423 K (1150 °C) with a strain rate of 10 s⁻¹ after a strain of 1. In the last phase, as will be shown in Section III–E, the strain rate and strain are estimated to be 18.5 s⁻¹ and 12.95, respectively. Thus, comparing the thermomechanical condition of the last phase with those of Brand et al. study,[41] it is reasonable to presume that the temperature increase in the final stage is due to plastic work. Finally, as the high-temperature interface material was extruded to the sides, the temperature decreased.

Because of material removal due to wear, material extrusion, and severe plastic deformation, measurement of the interface temperature by embedded thermocouple during LFW is almost impossible. However, the peak interface temperature can be estimated by extrapolation of the peak temperature data vs location from interface, as shown in Figure 10. According to this figure, the
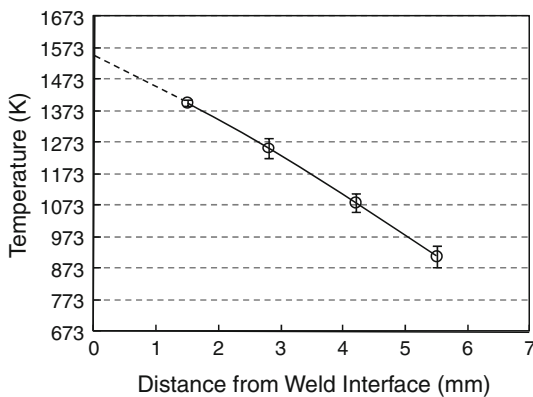

Fig. 10—Variation of the peak temperature as a function of distance from the interface in W4. The standard deviations of measurements are shown as error bars.

temperature of the interface can be of the order of 1553 K (1280 °C), which is in the range of the solidus temperature of the alloy, 1603 K (1330 °C). Soucail and Bienvenue[42] measured a temperature of 1553 K (1280 °C) at the weld metal interface during IFW of ASTROLOY.† Also, Kyusojin et al.[43] reported that,

---

†ASTROLOY is a trademark of General Electric Company, Fairfield, CT.

---

during IFW of S15C carbon steel, the temperature of the interface material reached 1553 K (1280 °C), which is 338 K (65 °C) below the solidus temperature of the alloy and very close to the difference between solidus temperature and extrapolated LFW temperature of the current study on WASPALOY, i.e., 323 K (50 °C). This indicates that, in friction welding processes, the interfacial material needs to be exposed to a high temperature, 323 to 333 K (50 to 60 °C) below the solidus, to have enough softening and plasticization.

The interface temperature can also be approximated by heat transfer analytical methods. According to a one-dimensional transient-heat-conduction analysis,[44] the temperature (T) at different locations (y) from interface as a function of time (t) is

$$T(y, t) = T_0 + \frac{2q_0 \sqrt{\frac{\alpha t}{\pi}}}{\lambda} \exp\left(-\frac{y^2}{4\alpha t}\right) - \frac{q_0 y}{\lambda}\left(1 - \text{erf}\left(\frac{y}{2\sqrt{\alpha t}}\right)\right) \quad [2]$$

where T_0, q_0, α, λ, and erf are, respectively, the room temperature, heat input, thermal diffusivity, thermal conductivity, and error function. Thermal diffusivity is normally expressed as

$$\alpha = \frac{\lambda}{p c_p} \quad [3]$$

In the preceding equation, p and c_p are, respectively, the density and heat capacity. The values for λ, p, and c_p are 11 W/(m·K), 8138 Kg/m³, and 520 J/(kg·K) for WASPALOY, respectively.[45] Therefore, α was calculated to be 2.60×10^{-6} m²/s. To ensure the accuracy of Eq. 2, initially, the calculated temperature by this equation after 4.4 seconds (end of the burn-off phase) was compared with the measured one from the thermocouple located at 1.5 mm. Considering q_0 = SPI = 3438 kW/m², the calculated and measured values were, respectively, 1228 and 1273 K (955 and 1000 °C), indicating a good agreement between the analytical and measured values. On this basis, the temperature at the interface (y = 0) 4.4 seconds after the start of the test was estimated to be 1493 K (1220 °C) at the end of the burn-off phase. Assuming that the temperature increase caused by plastic work is about 319 K (46 °C), as mentioned previously, and adding this temperature to the calculated one, the peak temperature at the interface could be estimated as 1540 K (1266 °C), which is very close to the extrapolated value, i.e., 1553 K (1280 °C). Therefore, it can be concluded that either

the extrapolation or one-dimensional transient-heat-conduction analysis is reliable for the prediction of the interface temperature in the LFW process. Also, other researchers[46] have reported that friction welding processes could be analyzed considering one-dimensional finite element analysis due to short time frictional heating and uniform heat generation across the interface.

E. *Variation in γ Grain Size across the Weld*

The material at the interface experiences rapid exposure to high temperatures, heavy deformation during LFW, and a fast cooling rate after welding. Accordingly, there is a significant temperature and strain gradient across the weld, leading to severe variations in microstructure and, consequently, mechanical properties. The EBSD maps of the γ matrix grains from regions adjacent to the joint interface, at 0.18 and 0.36 mm from the interface, and within the base metal are presented in Figure 11. The inverse pole figure, shown in this figure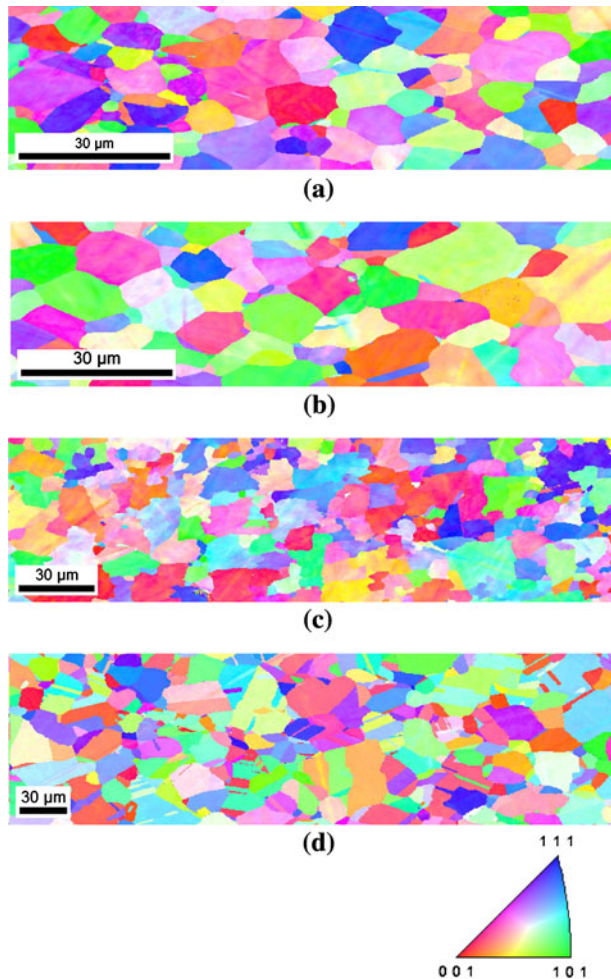, indicates the directions normal to the polished surface, which are [111], [001], and [101] for blue, red, and green grains, respectively. The variation of grain size obtained from EBSD studies is shown in Figure 12.

From the preceding results, it was determined that, at 0.9 mm from the weld interface and further, γ grain size remained almost constant and was about the same as that of the base metal (15.1 μm on average). In contrast, in areas limited to a distance of ±0.9 mm from the weld interface, the grain size decreased progressively from 15.1 to 7.5 μm at the weld interface. Such grain size evolution also has been observed by other authors. For example, Roder *et al.*[18] reported that, in inertial friction welded INCONEL 718, the base metal grains were reduced from 10 to 15 μm to 3 to 5 μm at the weld interface.

Previous studies[47] have indicated that TMP of WASPALOY in the temperature range of 1223 to 1453 K (950 to 1180 °C) results in dynamic recovery and DRX, depending on the amount of strain and strain rate. In due consideration of the LFW process, the region confined to ±0.9 mm from the weld interface experienced significant increase in temperature, strain, and strain rate (1.2 mm shortening for W4). According to the OM studies, the stationary and oscillating weld parts exhibited equal amounts of shortening in the case of W4. Thus, the initial position of 1.5 mm, which was the initial location of the closest thermocouple to the interface, was equivalent to a final position of 0.9 mm in the welded assembly. Temperature measurement and analysis made in the present study indicated that from the interface to 0.9-mm location, the peak temperature was at least 1400 K (1126 °C) for SPI of 3438 kW/m^2. The maximum local strain rate ($\dot{\varepsilon}$) in the weld area was calculated using the analytical equation proposed by Vairis and Frost,[16]

$$\dot{\varepsilon} = \frac{af}{L} \qquad [4]$$

to be 18.5 s^{-1}. By multiplying the forge time (0.7 seconds) by the calculated strain rate, the average strain in the weld area could be estimated to be 12.95 for the W4 specimen. The following equation proposed
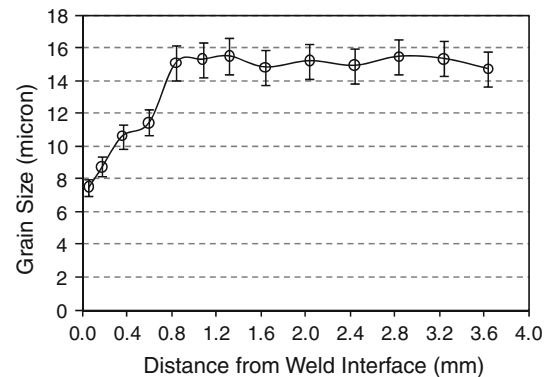

Fig. 11—EBSD map of the W4 sample: (*a*) adjacent to the weld interface; (*b*) and (*c*) at 0.18 and 0.36 mm, respectively, from the weld interface; and (*d*) base metal.

Fig. 12—Grain size at various locations from the weld interface in the W4 specimen.

by Shen et al.[29] was used for estimating the critical strain (ε_c) for DRX:

$$\bar{\varepsilon}_p = 1.685x10^{-4}d_o^{0.54}\left[\dot{\varepsilon}\exp\left(\frac{468,000}{8.31T}\right)\right]^{0.106} \text{ (Supersolvus)}$$

[5]

where $\bar{\varepsilon}_p$ is the strain at peak stress in the true stress-strain curve obtained from the hot compression test. Assuming $\varepsilon_c = 0.8\bar{\varepsilon}_p$, the critical strain for the onset of DRX at 1400 K (1126 °C) was estimated to be about 0.10 for an initial grain size (d_0) of 15.1 μm and strain rate of 18.5 s^{-1}. Therefore, it can be reasonably assumed that DRX was operating during the LFW of WASPALOY at the interface and its proximity. In terms of creep, DRX leading to grain refinement may be problematic, but grains could be coarsened by heat treatment. On the other hand, the occurrence of DRX in the weld area is beneficial as the absence of microcracking observed in the linear friction welded WASPALOY samples of the current study may be related to the DRX. Indeed, microcracking observed in fusion welded WASPALOY, INCONEL 718, and Allvac 718 Plus‡[5,6]

---

‡Allvac 718 Plus is a trademark of Allegheny Technologies Inc. (ATI), Monroe, NC.

---

has been reported to be a result of grain boundary liquation in the HAZ. The phenomenon has been associated with the formation of low melting point compounds at the grain boundary. The tensile stresses that are active in the solid part of the HAZ during the solidification of the liquid weld metal open these grain boundaries.[5] By contrast, during LFW, as DRX takes place in the TMAZ, the rapid grain boundary migration does not allow major changes in the composition of the grain boundary and eliminates the possible formation of low melting point compounds.

Referring back to the grain size analysis, at a distance of 0.9 mm from the weld interface and beyond, the γ grain size constancy, as shown in Figure 12, may be related to two factors: (1) pinning of grain boundaries due to the presence of γ', which resulted in the inhibition of DRX; and (2) process parameters such as temperature and strain not being high enough to initiate DRX. For example, at the final position of 2.2 mm from the weld interface, the peak temperature was measured to be 1257 K (984 °C), which is below the γ' solvus as well as the minimum DRX temperature of WASPALOY, i.e., 1273 K (1000 °C).

Between 0.9 mm and the weld interface, both γ grain size and hardness decreased (Figures 4 and 12), while according to the Hall–Petch equation, the yield strength, and generally hardness, increases with decreasing grain size. The obtained results indicate that other microstructural features are contributing to the hardness evolution, as discussed further subsequently.

At the end of this section, it should be added that, according to Figure 11, no preferred orientation of the grains was observed from the base metal to the interface.
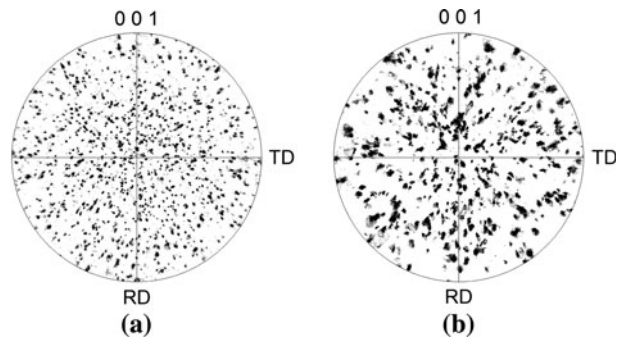

Fig. 13—(001) pole figures: (a) base metal and (b) near the weld interface in W4.

In fact, as shown in Figure 13(a), the base metal exhibited a random texture as a consequence of DRX and breaking up of the microstructure during the TMP of the as-received disc. Similarly, a random texture in the weld area (Figure 13(b)) was observed due to the occurrence of the further DRX during LFW.

F. Variation in γ' Size and Volume Fraction across the Weld

Figure 14 shows high magnification FEG-SEM images of γ' in the base metal, at various locations from the weld and at the weld interface of W4. The distribution of γ' precipitates presented in Figure 15 revealed a bimodal distribution in the unaffected base metal. In the base metal, primary γ' precipitates, 193 to 297 nm in size (average 250 nm), and secondary globular γ' precipitates, 12 to 88 nm in size (average 43 nm), were present (Figure 14(a)). Other researchers[48] have also reported a bimodal γ' distribution in WASPALOY after standard heat treatment with average sizes of 280 and 50 nm. It has been reported that[1,49] the chemical composition of the primary γ' particles is different from that of the secondary ones, to some extent. The levels of Al and Ti are higher in the primary precipitates relative to the secondary ones, whereas the reverse situation exists for Cr, Co, and Mo.

The base metal contained about 6 ± 2 vol pct primary and 27 ± 5 vol pct secondary γ' precipitates and, consequently, a total volume fraction of 33 ± 4 pct precipitates. This finding is in agreement with the generally reported value of 30 vol pct γ' in WASPALOY.[7] The secondary γ' precipitates constituted a high volume fraction (82 pct) of the total γ' in the γ matrix. This is probably the main factor for the observed high hardness (426 HV) of the base metal.

Considering Figure 14, dramatic variations in the γ' characteristics occurred in the TMAZ during LFW. Moving from the base metal to the weld interface, most of the secondary γ' began to dissolve. At 0.9 mm from the weld, all the secondary γ' was dissolved leaving only partially dissolved primary γ'. At the interface, virtually no γ' particles were observed. The few retained precipitates at the interface were characterized by EDS to be Ti and Cr carbides, MC type carbides, that are normally stable at temperatures close to the melting point of the
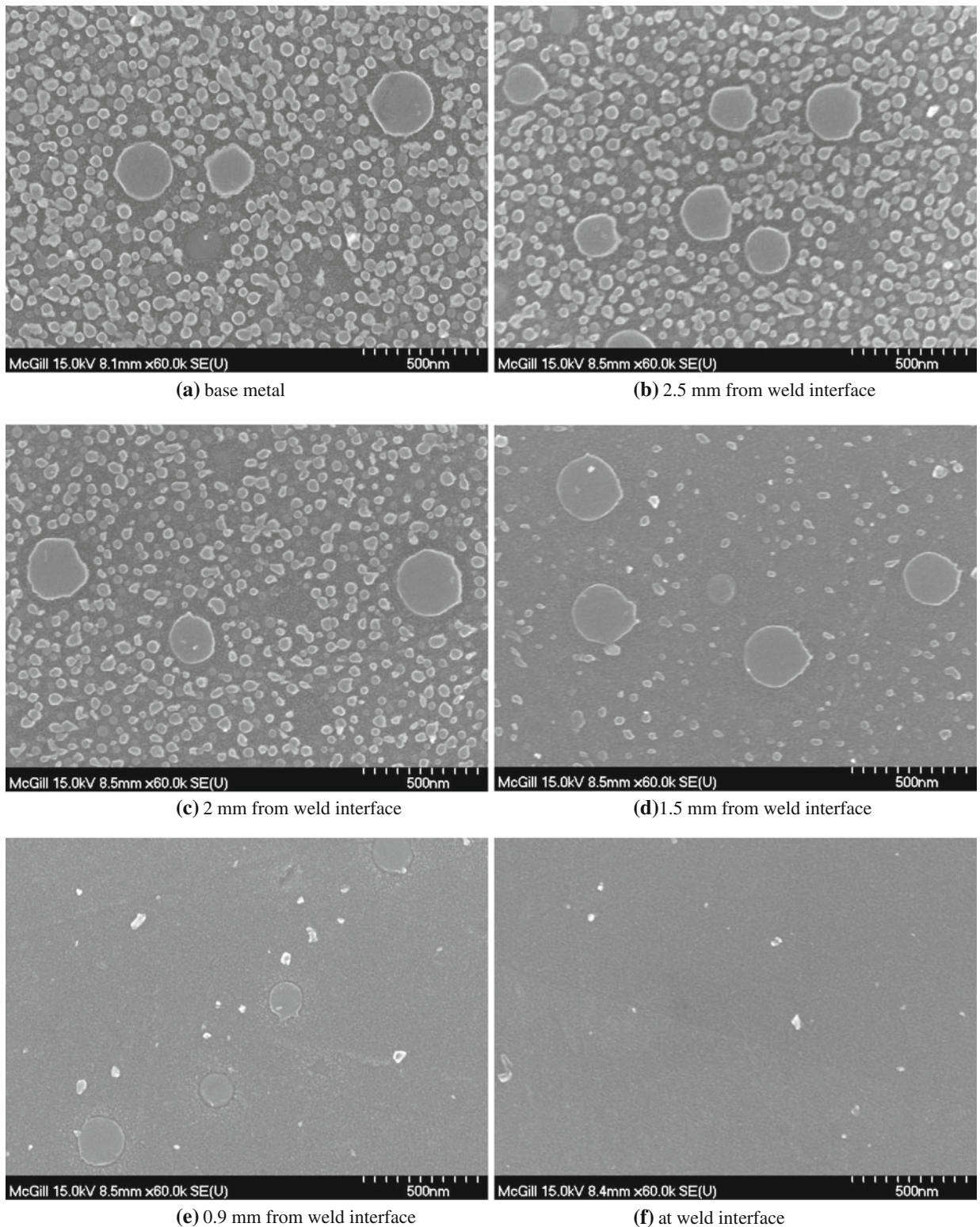
(a) base metal

(b) 2.5 mm from weld interface

(c) 2 mm from weld interface

(d) 1.5 mm from weld interface

(e) 0.9 mm from weld interface

(f) at weld interface

Fig. 14—FEG-SEM images of γ' in W4: (*a*) in the base metal; (*b*) through (*e*) at 2.5, 2.0, 1.5, and 0.9 mm, respectively, from the weld; and (*f*) at the weld interface.

alloy.[50] Carbides were also present at the base metal as well as other locations from the weld interface.

Therefore, the interface material mostly consisted of supersaturated γ phase with γ' forming elements such as Al, Ti, Cr, Mo, and Co. To have a better understanding of the γ' dissolution evolution, the variation in γ' volume fraction across the TMAZ is illustrated in Figure 16. The primary γ' volume fraction started to decrease
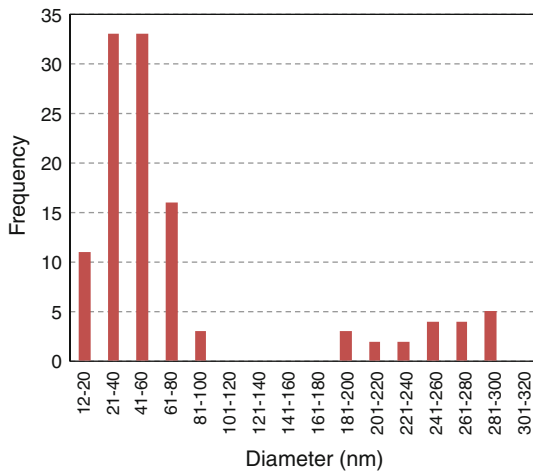
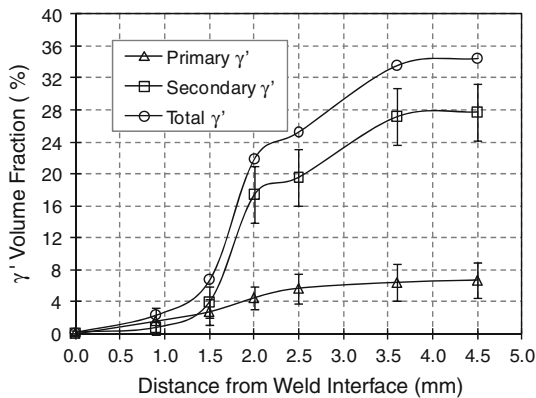Fig. 15—Distribution of γ′ precipitates in the unaffected base metal in the W4 specimen.

Fig. 16—Variation in γ′ volume fraction as a function of position from the weld interface in W4. The 95 pct confidence intervals[34] for volume fraction determinations are shown as error bars.
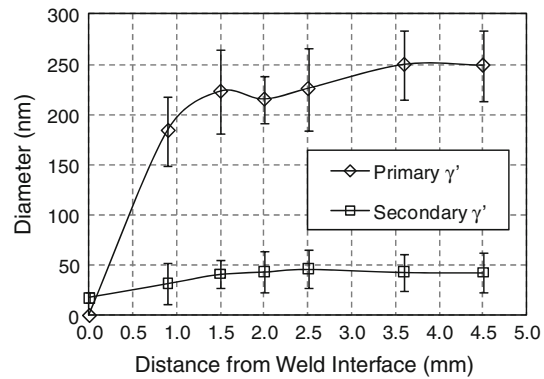

Fig. 17—Average γ′ diameter at different locations from the interface in W4. The standard deviations of measurements are shown as error bars.

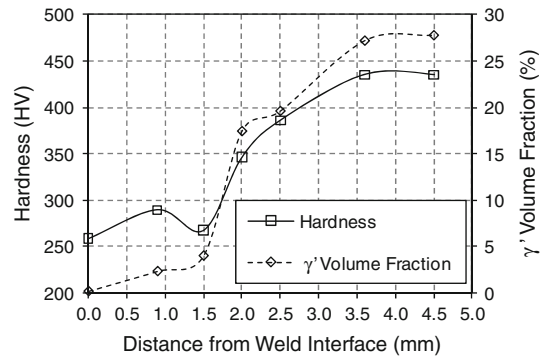Fig. 18—Variation of hardness and γ′ volume fraction vs distance from the interface.

gradually at 2.5 mm from the interface. In contrast, the secondary γ′ content began to decrease from 3.6 mm, while the rate of decrease was significant from 3.6 to 2.5 mm and from 2.0 to 1.5 mm. This finding clearly indicates that secondary γ′ began to dissolve first. The trend of the total γ′ volume fraction was similar to that of the secondary γ′ as secondary precipitates constituted 82 pct of the total γ′ content of the base metal.

Comparing the start position for γ′ dissolution with the temperature profile (Figure 10), the start temperatures for primary and secondary γ′ dissolutions were 1283 and 1153 K (1010 °C and 880 °C), respectively. Soucail and Bienvenue[42] indicated that the start temperature for secondary γ′ dissolution with average size of 10 nm is in the 1073 to 1123 K (800 to 850 °C) range. The difference between the start temperatures of the primary and secondary γ′ dissolution can be attributed to the difference in their chemical composition.

The variation in the diameter of γ′ precipitates at different locations from the interface is shown in Figure 17. For all positions far from 0.9 mm from the interface, the primary γ′ average size lay above 200 nm.

At 0.9 mm, where primary γ′ particles were partially dissolved (Figure 14(e)), the size decreased to 184 ± 35 nm. At the interface, all primary particles were in solution (Figure 14(f)). For secondary γ′, there were no significant changes in size from the base metal to the 1.5-mm position, but from there toward the interface, the secondary γ′ size decreased gradually due to dissolution of these particles.

G. Relationships of γ′ and MC Carbide Evolution with Hardness Profile

It has been reported that γ′ precipitates above 200-nm diameter are less effective in increasing the hardness.[51] Therefore, to correlate the γ′ dissolution to the hardness profile, only the volume fraction of secondary γ′ was considered. Nevertheless, for 0.9 mm, where the average primary particle size was lower than 200 nm, the volume fractions of the primary and secondary γ′ particles were added together. The resultant volume fraction profile is superimposed on the hardness profile in Figure 18. It can be seen that the overall γ′ volume fraction correlates well with the hardness profile from the base metal (4.5 mm) to the 1.5-mm location, where there was a significant decrease in γ′ volume fraction and, consequently, hardness. In the interval of 1.5 to 0.9 mm, the γ′ content continued to decrease while the hardness
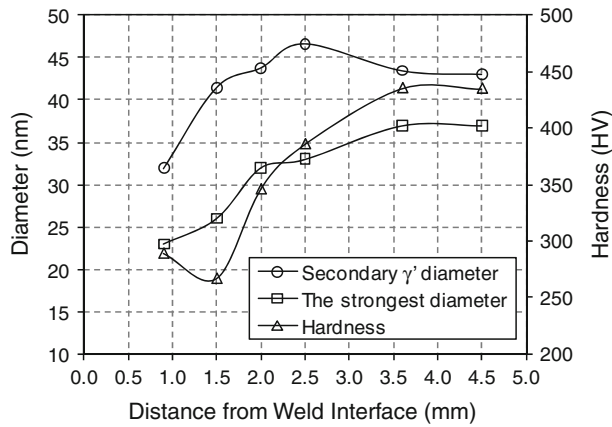
Fig. 19—Secondary γ' diameter, the strongest diameter derived from Ref. 54, and hardness as a function of position from interface.
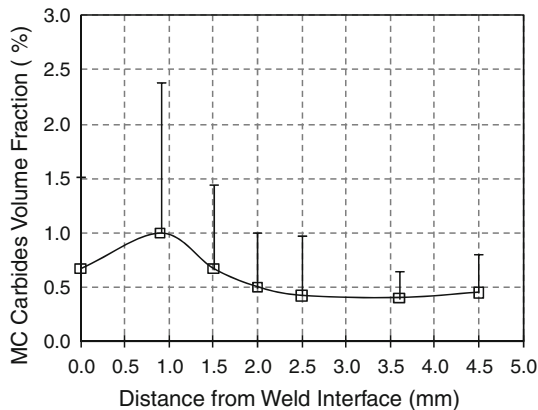

Fig. 20—Variation of MC carbide content with location from the weld interface in W4. The average 95 pct confidence intervals[34] for volume fraction determination are shown as error bars.

Fig. 21—Variation of MC carbide size with position in W4. The standard deviations of measurements are shown as error bars.

increased by about 22 HV. Although the γ' volume fraction and morphology essentially dictate the hardness,[52] other factors such as carbide volume fraction probably influenced this behavior. It is not believed that γ grain size had any significant influence on the hardness profile, since the γ grain size did not notably change from 1.5 to 0.9 mm (Figure 12).

The influence of γ' size on the hardness of nickel-base alloys was studied by Reppich et al.[53] They found that maximum hardness occurs when the γ' size is such that there is the highest level of resistance against cutting of precipitates by weakly coupled dislocation pairs. Jackson et al.[54] also reported that, to obtain the highest hardness, a size large enough for cutting by strongly coupled dislocation pairs is desirable and the maximum value of the critical resolved shear stress (CRSS) is at the transition point between cutting by weakly and strongly coupled dislocations. At large particle size (>200 nm), Orowan looping occurs and the hardness decreases.[25]

The strongest particle size that depends on the secondary γ' volume fraction was derived from the methodology presented in Reference 54, and the results are shown in Figure 19 along with the measured hardness and secondary γ' size values. At 2.5- and
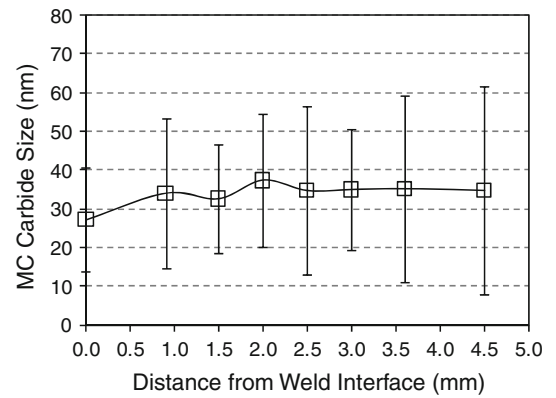
1.5-mm positions, a significant deviation from the strongest size relative to the base metal (4.5-mm location) is observed, which, based on the preceding discussion, could influence the hardness drop. By contrast, at 0.9 mm, approaching the strongest γ' size may have caused an increase in the hardness.

The variation in volume fraction of MC carbides as a function of location from the interface is presented in Figure 20. At the 0.9-mm location, where higher hardness values were measured, the carbide volume fraction was the highest. Indeed, significant γ' dissolution at 0.9 mm relative to the base metal (Figure 16) can provide Ti for precipitation of TiC. Carbon might be provided from soluble carbon in the alloy matrix or from dissolution of $M_{23}C_6$ carbides, since $M_{23}C_6$ is entirely in solution at temperatures above 1283 K (1010 °C).[50] Thus, carbide precipitation might have been an additional factor for the high hardness values observed at 0.9 mm. At the interface where all γ' was dissolved, there should be a high possibility for MC carbide precipitation since more Ti was provided. However, as shown in Figure 8, the cooling rate increased with movement toward the interface, probably due to the flash development and heat dissipation into the surroundings. Therefore, less MC carbide precipitation occurred at the interface compared to the 0.9-mm position, since carbide precipitation is a diffusion type process and enough time for diffusion was not available at the interface.

The MC carbide size distribution as a function of position from the interface is shown in Figure 21 for W4. In contrast to γ', the variation in MC size with position was not considerable and these particles were very stable. MC particles contributed to the hardness of the alloy since their sizes lay in the 30- to 35-nm range from the interface to the base metal. However, since their volume fraction was low, γ', with a high volume fraction, was the main strengthening phase in the base metal.

Considering the hardness profile and γ' volume fraction evolution across the TMAZ (Figure 18), the continuous dissolution of the γ' correlates to the continuous decrease in the hardness from the 0.9-mm position to the weld interface. In fact, at the interface,
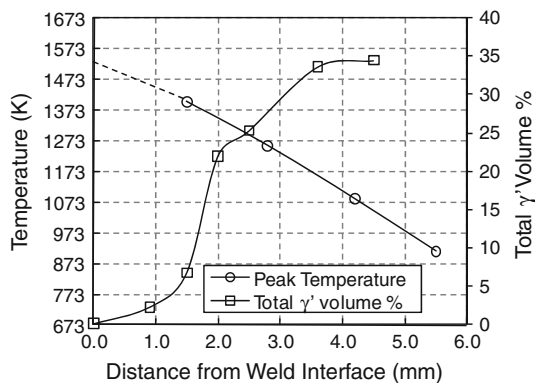
Fig. 22—Variation of peak temperature and total γ' volume fraction as a function of location from the weld interface.

the hardness dropped to the value of the solution heat-treated condition that is reported[55,56] to be 230 to 266 HV. This confirmed full dissolution of γ' at the weld interface.

H. *Temperature and γ' Dissolution*

The temperature measurement results are superimposed on the γ' volume fraction in Figure 22. At the weld interface, where the temperature was the highest, the dissolution of the γ' precipitates was the greatest and, consequently, the hardness was the lowest. With increasing distance from the weld interface, the peak temperature decreased and, consequently, the rate of γ' dissolution decreased.

During TMP, γ' starts to dissolve as temperature increases. Once a temperature beyond γ' solvus is reached, full γ' dissolution occurs. Complete γ' dissolution at the interface indicated that the interface experienced temperatures higher than the γ' solvus, *i.e.*, 1303 K (1030 °C). However, the heating rate can influence the γ' solvus. In a previous study,[57] the influence of the heating rate on the γ' solvus was investigated for constant holding time of 0.5 seconds and cooling rate of 80 K/s. Based on this study, an increase in the heating rate from 0.01 to 300 K/s would shift the primary and secondary γ' solvus to higher temperatures by 400 and 300 K (126 and 26 °C), respectively. Therefore, the interface material experienced a temperature higher than the summation of the γ' solvus temperature and the heating rate effect, *i.e.*, higher than 1433 K (1160 °C).

I. *γ' Reprecipitation at the End of the LFW Process*

The rapid γ' reprecipitation at the end of welding during the cooling phase of the process could result in microcracking in the HAZ by inducing large shrinkage stresses.[58] Figure 16 suggests that no γ' repreciptation occurred at the interface from the supersaturated solution. The possible precipitation of very fine γ' at the weld interface was investigated using TEM. The examination did not reveal any reprecipitated γ' at the interface (Figure 23). It is believed that the fast cooling rate (62 ± 4 K/s) at the end of the LFW process and the
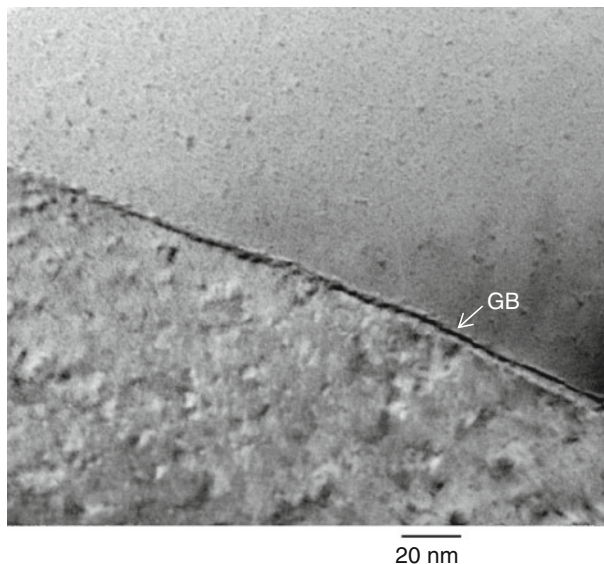

Fig. 23—TEM image of the weld interface in the W4 specimen. The grain boundary (GB) is shown with an arrow.

low (Ti + Al) content of WASPALOY with respect to other nickel-base superalloys have resulted in lack of repreciptation at the interface. Therefore, the lack of γ' repreciptation on the cooling cycle from the welding temperature might be another factor contributing to the lack of microcracking in the linear friction welded WASPALOY in addition to the DRX.

At the end, it is worth comparing the evolution of γ' characteristics obtained in the present work with those reported in the literature. Preuss *et al.*[39] reported that during friction welding of alloys with low precipitate content, such as INCONEL 718 (25 pct γ'/γ''), full γ' dissolution without repreciptation at the end of welding occurred within 1 mm of the weld, reflected by a hardness drop from 430 HV (base metal) to 270 HV. In contrast, in the case of alloys such as ASTROLOY and UDIMET§ 720Li with high γ' content (~50 to

---

§UDIMET is a trademark of Special Metals Corporation, New Hartford, NY.

---

60 pct), they found a high tendency for repreciptation of γ' at the end of friction welding resulting in a hardness peak in the TMAZ. Also, no γ' repreciptation was identified in the fusion zone of laser and electron beam welded WASPALOY, with a power input similar to the one used in the current study.[7] This indicates that, in low γ' content WASPALOY, γ' repreciptation is inhibited because of the very high cooling rate in laser and electron beam welding processes. In contrast, in the weld area of laser and electron beam welded UDIMET 720Li, a high γ' containing alloy, for the same power input, very fine γ' was revealed by TEM studies. Thus, it could be concluded that re-precipitation of γ' at the end of friction welding or fusion welding is a compromise between the volume fraction of γ' in the material and the cooling rate at the end of the process. The higher the

cooling rate or the lower the γ' content, the lower would be the tendency for γ' reprecipitation.

IV. SUMMARY AND CONCLUSIONS

The LFW behavior of WASPALOY was studied under different processing conditions. Microstructure characterization and mechanical property evaluation were carried out across the weld. The processing conditions with a frequency of 80 Hz, amplitude of 3 mm, and a pressure of 90 MPa resulted in a reproducible sound joint free from pores and microcracks. For this LFW condition, the TMAZ width was 3.3 mm on either side of the weld interface and there was an overall loss of strength from 426 to 258 HV. At 0.9 mm from the weld interface, a temperature as high as 1400 K (1126 °C) was experienced during LFW. This temperature condition along with the introduction of large amounts of plastic deformation at very high strain rate encouraged DRX in an area confined to 0.9 mm from the weld such that the grain size of the base metal was refined from 15.1 to 7.5 μm at the interface. The incidence of DRX during LFW is useful in inhibiting microcracking in the weldment. The gradual γ' dissolution from the base metal to the weld interface caused a progressive decrease in the hardness. The absence of γ' reprecipitation at the end of the welding, during the cooling phase, may be another factor contributing to the lack of microcracking in the linear friction welded WASPALOY. All LFW tensile tests failed from the weld extremities due to the presence of metal oxides and weak bonding at the periphery of the weldment. An increase in the axial shortening to above 1.2 mm should allow extrusion of all the oxides from the interface to the sides as flash and increase the bonded area at the weld interface.

ACKNOWLEDGMENTS

REFERENCES

1. Y.C. Fayman: *Mater. Sci. Eng.*, 1986, vol. 82, pp. 203–15.
2. A.A. Guimaraes: M.Sc. Thesis, McGill University, Montreal, 1980, pp. 1–2.
3. M.E. Nunn: *1st Int. Conf. on Innovation and Integration in Aerospace Sciences*, CEIAT, Northern Ireland, United Kingdom, 2005.
4. Z.W. Huang, H.Y. Li, M. Preuss, M. Karadge, P. Bowen, S. Bray, and G. Baxter: *Metall. Mater. Trans. A*, 2007, vol. 38A, pp. 1608–20.
5. P. Adam: *Welding of High Strength Gas Turbine Alloys*, Applied Science Publisher Ltd., London, 1978, pp. 737–68.
6. K.R. Vishwakarma, N.L. Richards, and M.C. Chaturvedi: *6th Int. Symp. on Superalloys 718, 625, 706 and Derivatives*, E.A. Loria, ed, TMS, Pittsburgh, PA, 2005, pp. 637–47.
7. N.C. Sekhar and R.C. Reed: *Sci. Technol. Weld. Join.*, 2002, vol. 7, pp. 77–87.
8. T.J. Ma, W.-Y. Li, Q.Z. Xue, Y. Zhang, J.L. Li, and S.Q. Yang: *Mater. Sci. Forum*, 2008, vols. 580–582, pp. 405–08.
9. H.Y. Li, Z.W. Huang, S. Bray, G. Baxter, and P. Bowen: *Mater. Sci. Technol.*, 2007, vol. 23, pp. 1408–18.
10. S.W. Kallee, E.D. Nicholas, and M.J. Russell: *10th World Conf. on Titanium*, G. Lütjering and J. Albrecht, eds., Wiley VCH, Germany, 2003, pp. 2867–74.
11. K. Asokkumar: *WRI J.*, 2003, vol. 24, pp. 12–20.
12. A. Vairis and M. Frost: *Mater. Sci. Eng. A*, 2000, vol. 292, pp. 8–17.
13. H. Seli, I.A.Md. Ismail, E. Rachman, and Z.A. Ahmad: *J. Mater. Process. Technol.*, 2010, vol. 210, pp. 1209–16.
14. I. Hulea, P. Hoffmann, M. Brinza, D.R. Batchelor, and D. Schmeisser: *2nd Int. Symp. on Aluminum Surface Science and Technology*, Manchester, England, Emerald Group Publishing Limited, Bingley, United Kingdom, 2000, pp. 157–62.
15. "Resistance and Solid-State Welding," http://www.ewi.org/capabilities/rssw.asp.
16. A. Vairis and M. Frost: *Wear*, 1998, vol. 217, pp. 117–31.
17. "Linear Friction Welding of Blisks for Power Generation," http://www.twi.co.uk/j32k/unprotected/band_1/power_linearfric.html.
18. O. Roder, D. Helm, S. Neft, J. Albrecht, and G. Luetjering: *6th Int. Conf. on Superalloys 718, 625, 706 and Derivatives,* O. Roder, D. Helm, S. Neft, J. Albrecht, and G. Luetjering, eds., TMS, Warrendale, PA, 2005, pp. 649–59.
19. W.A. Baeslack, T.F. Broderick, M. Juhas, and H.L. Fraser: *Mater. Charact.*, 1994, vol. 33, pp. 357–67.
20. M. Karadge, M. Preuss, P.J. Withers, and S. Bray: *Mater. Sci. Eng. A*, 2008, vol. 491, pp. 446–53.
21. P.L. Threadgill: *Stainless Steel World*, 1996, vol. 88, pp. 65–67.
22. R.E. Bailey: *2nd Int. Conf. on Superalloys—Processing*, Seven Springs, PA, Battelle Columbus Labs., Columbus, OH, 1972, pp. J1–J21.
23. C.T. Sims, N.S. Stoloff, and W.C. Hagel: *Superalloys II*, John Wiley & Sons, New York, NY, 1987, pp. 66–78.
24. M.R. Winstone and J.W. Brooks: *Ciência Technol. Mater.*, 2008, vol. 20, pp. 15–24.
25. M. Preuss, J.W.L. Pang, P.J. Withers, and G.J. Baxter: *Metall. Mater. Trans. A*, 2002, vol. 33A, pp. 3215–25.
26. C. Mary and M. Jahazi: *Adv. Mater. Res.*, 2007, vols. 15–17, pp. 357–62.
27. C. Mary and M. Jahazi: *Adv. Eng. Mater.*, 2008, vol. 10, pp. 573–78.
28. N.W. Bonner and A.N. Ezeilo: *6th Int. Conf. on Residual Stresses*, G.A. Webster, ed., Oxford, United Kingdom, Institute of Materials, London, 2000, pp. 1385–92.
29. G. Shen, S.L. Semiatin, and R. Shivpuri: *Metall. Mater. Trans. A*, 1995, vol. 26A, pp. 1795–803.
30. P. Wanjara and M. Jahazi: *Metall. Mater. Trans. A*, 2005, vol. 36A, pp. 2149–64.
31. E. Dalgaard, M. Jahazi, and J.J. Jonas: *Friction Stir Welding and Processing—V,* TMS 2009 Annual Meeting & Exhibition, R.S. Mishra, M.W. Mahoney, and T.J. Lienert, eds., TMS, San Francisco, CA, 2009, pp. 55–64.
32. S. Xu, J.I. Dickson, and A.K. Koul: *Metall. Mater. Trans. A*, 1998, vol. 29A, pp. 2687–95.
33. B. Lindsley and X. Pierron: *Superalloys 2000*, T.M. Pollock, R.D. Kissinger, R.R. Bowman, K.A. Green, M. McLean, S. Olson, and J.J. Schirra, eds., TMS, Warrendale, PA, 2000, pp. 59–68.
34. ASTM Standard E 562-02, *Annual Book of ASTM Standards*, ASTM, Philadelphia, PA, 2002, vol. 3 (1), pp. 1–7.
35. T.J. Ma, W.-Y. Li, and S.Y. Yang: *Mater. Des.*, 2009, vol. 30, pp. 2128–32.
36. W.-Y. Li, T.J. Ma, S.Q. Yang, Q.Z. Xu, Y. Zhang, J.L. Li, and H.L. Liao: *Mater. Lett.*, 2008, vol. 62, pp. 293–96.
37. E.D. Nicholas and W.M. Thomas: *Int. J. Mater. Prod. Technol.*, 1998, vol. 13, pp. 45–55.

38. H.H. Koo and W.A. Baeslack: *Mater. Charact.*, 1992, vol. 28, pp. 157–64.
39. M. Preuss, P.J. Withers, and G.J. Baxter: *Mater. Sci. Eng. A*, 2006, vol. 437, pp. 38–45.
40. B. Grant, M. Preuss, P.J. Withers, G. Baxter, and M. Rowlson: *Mater. Sci. Eng. A*, 2009, vols. 513–514, pp. 366–75.
41. A.J. Brand, K. Karhausen, and R. Kopp: *Mater. Sci. Technol.*, 1996, vol. 12, pp. 963–69.
42. M. Soucail and Y. Bienvenu: *Mater. Sci. Eng. A*, 1996, vol. 220, pp. 215–22.
43. A. Kyusojin, K. Nishimoto, Y. Otobe, S. Kanai, and Y. Ogasawara: *Bull. Jpn. Soc. Mech. Eng.*, 1980, vol. 23 (182), pp. 1388–95.
44. W.-Y. Li, T. Ma, and S. Yang: *Adv. Eng. Mater.*, 2010, vol. 12 (1–2), pp. 35–43.
45. Technical Data Sheet, Carpenter Technology Corporation, Wyomissing, PA, 2006.
46. M. Maalekian, E. Kozeschnik, H.P. Brantner, and H. Cerjak: *Acta Mater.*, 2008, vol. 56, pp. 2843–55.
47. A.A. Guimaraes and J.J. Jonas: *Metall. Trans. A*, 1981, vol. 12A, pp. 1655–66.
48. S.-F. Toh and W.M. Rainforth: *Mater. Sci. Technol.*, 1996, vol. 12, pp. 1007–14.
49. D. Blavette, A. Bostel, and J.M. Sarrau: *Metall. Trans. A*, 1985, vol. 16A, pp. 1703–11.
50. G.P. Sabol and R. Stickler: *Phys. Status Solidi*, 1969, vol. 35, pp. 11–52.
51. H. Monajati, M. Jahazi, R. Bahrami, and S. Yue: *Mater. Sci. Eng. A*, 2004, vol. 373, pp. 286–93.
52. M. Durand-Charre: *The Microstructure of Superalloys*, CRC Press, Amsterdam, 1997, pp. 68–69.
53. B. Reppich, P. Schepp, and G. Wehner: *Acta Metall.*, 1982, vol. 30, pp. 95–104.
54. M.P. Jackson and R.C. Reed: *Mater. Sci. Eng. A*, 1999, vol. 259, pp. 85–97.
55. *Waspaloy*, Publication Number SMC-011, Special Metals Corporation, New Hartford, NY, Sept. 2004.
56. Z. Li, S.L. Gobbi, and J.H. Loreau: *J. Mater. Process. Technol.*, 1997, vol. 65, pp. 183–90.
57. M. Soucail, A. Moal, L. Naze, E. Massoniz, C. Levaillant, and Y. Bienvenu: in *Superalloys 1992*, S.D. Antolovich, R.W. Stusrud, R.A. Mackay, D.L. Anton, T. Khan, R.D. Kissinger, and D.L. Klarstrom, eds., TMS, Warrendale, PA, 1992, pp. 847–56.
58. O.A. Ojo and M.C. Chaturvedi: *Mater. Sci. Eng. A*, 2005, vol. 403, pp. 77–86.